

























## Radio afterglows from tidal disruption events: An unbiased sample from ASKAP RACS

AKASH ANUMARLAPUDI <sup>1</sup> DOUGAL DOBIE <sup>2,3</sup> DAVID L. KAPLAN <sup>1</sup> TARA MURPHY <sup>4,3</sup> ASSAF HORESH <sup>5</sup>  
EMIL LENC <sup>6</sup> LAURA DRIESSEN <sup>4</sup> STEFAN W. DUCHESNE <sup>7</sup> HANNAH DYKAAR <sup>8,9</sup> B. M. GAENSLER <sup>10,8,9</sup>  
TIMOTHY J. GALVIN <sup>7,11</sup> JOE GRUNDY <sup>7,11</sup> GEORGE HEALD <sup>7</sup> AIDAN W. HOTAN <sup>7</sup> MINH HUYNH <sup>7</sup>  
JAMES K. LEUNG <sup>8,5</sup> DAVID MCCONNELL <sup>6</sup> VANESSA A. MOSS <sup>6,4</sup> JOSHUA PRITCHARD <sup>4,6,3</sup> WASIM RAJA,<sup>6</sup>  
KOVI ROSE <sup>4,6</sup> GREGORY SIVAKOFF <sup>12</sup> YUANMING WANG <sup>2,3</sup> ZITENG WANG <sup>11</sup> MARK H. WIERINGA,<sup>6</sup> AND  
MATTHEW T. WHITING <sup>6</sup>

<sup>1</sup>*Department of Physics, University of Wisconsin-Milwaukee, P.O. Box 413, Milwaukee, WI 53201, USA*

<sup>2</sup>*Centre for Astrophysics and Supercomputing, Swinburne University of Technology, Hawthorn, VIC 3122, Australia*

<sup>3</sup>*ARC Centre of Excellence for Gravitational Wave Discovery (OzGrav), Hawthorn, Victoria, Australia*

<sup>4</sup>*Sydney Institute for Astronomy, School of Physics, University of Sydney, NSW, 2006, Australia*

<sup>5</sup>*Racah Institute of Physics, The Hebrew University of Jerusalem, Jerusalem, 91904, Israel*

<sup>6</sup>*CSIRO Space and Astronomy, PO Box 76, Epping, NSW, 1710, Australia*

<sup>7</sup>*CSIRO Space and Astronomy, PO Box 1130, Bentley, WA, 6102, Australia*

<sup>8</sup>*Dunlap Institute for Astronomy and Astrophysics, University of Toronto, 50 St. George St., Toronto, ON M5S 3H4, Canada*

<sup>9</sup>*David A. Dunlap Department of Astronomy and Astrophysics, University of Toronto, 50 St. George St., Toronto, ON M5S 3H4, Canada*

<sup>10</sup>*Department of Astronomy and Astrophysics, University of California Santa Cruz, 1156 High Street, Santa Cruz, CA 95064, USA*

<sup>11</sup>*International Centre for Radio Astronomy Research - Curtin University, 1 Turner Avenue, Bentley, WA 6102, Australia*

<sup>12</sup>*Department of Physics, University of Alberta, CCIS 4-181, Edmonton AB T6G 2E1, Canada.*

### ABSTRACT

Late-time ( $\sim$  year) radio follow-up of optically-discovered tidal disruption events (TDEs) is increasingly resulting in detections at radio wavelengths, and there is growing evidence for this late-time radio activity to be common to the broad class of sub-relativistic TDEs. Detailed studies of some of these TDEs at radio wavelengths are also challenging the existing models for radio emission. Using all-sky multi-epoch data from the Australian Square Kilometre Array Pathfinder (ASKAP), taken as a part of the Rapid ASKAP Continuum Survey (RACS), we searched for radio counterparts to a sample of optically-discovered TDEs. We detected late-time emission at RACS frequencies (742-1032 MHz) in five TDEs, reporting the independent discovery of radio emission from TDE AT2019ahk and extending the time baseline out to almost 3000 days for some events. Overall, we find that at least  $22^{+15}_{-11}\%$  of the population of optically-discovered TDEs has detectable radio emission in the RACS survey, while also noting that the true fraction can be higher given the limited cadence (2 epochs separated by  $\sim$  3 years) of the survey. Finally, we project that the ongoing higher-cadence ( $\sim$  2 months) ASKAP Variable and Slow Transients (VAST) survey can detect  $\sim$  20 TDEs in its operational span (4 yrs), given the current rate from optical surveys.

*Keywords:* Radio transient sources (2008) — Tidal disruption (1696) — Extragalactic radio sources (508) — Radio continuum emission (1340) — Radio sources (1358)

### 1. INTRODUCTION

The discovery of tidal disruption events (TDEs; Rees 1988) thus far was initially dominated by X-ray surveys

(Halpern et al. 2004) and then by optical/ultraviolet (O/UV) surveys in more recent times (van Velzen et al. 2021; Hammerstein et al. 2023; Yao et al. 2023). At O/UV wavelengths, emission from TDEs has a characteristic blue continuum with hydrogen and/or helium

emission lines<sup>1</sup> and can be accurately modeled as a black body with temperatures peaking near UV wavelengths (Gezari 2021). Radio emission from TDEs, expected from the interaction of nascent jets or outflows, was initially detected only in a handful of TDEs and this initial sample was dominated by TDEs that were discovered at higher energies. It was estimated by Alexander et al. (2020) that not all TDEs result in radio detections, with only  $\sim 20\%$  of them being radio bright. The distribution of radio luminosities from this initial crop of TDEs indicated a dichotomy at radio wavelengths where the luminosity differed by 2–3 orders of magnitude (Alexander et al. 2020). The more luminous events resulted from relativistic jetted TDEs in which the radio luminosity exceeded  $10^{40}$  erg/s, while the less luminous events were from TDEs with sub-relativistic outflows where the isotropic radio luminosity were around  $10^{38}$  ergs/s (Zauderer et al. 2011; Alexander et al. 2016, 2020).

Shock-accelerated relativistic electrons produce radio emission from TDEs via the synchrotron mechanism (Alexander et al. 2020). This can be due to external shocks driven by jets/outflows or unbound stellar debris into the circumnuclear medium (CNM; Zauderer et al. 2011; Alexander et al. 2016; Krolik et al. 2016) or due to internal shocks within the jet (Pasham & van Velzen 2018). By modeling the spectral and temporal evolution of the emission, one can estimate the jet/outflow properties, particularly the velocity of the ejecta, their launch time relative to the optical flare, and the energy injected into the CNM (Granot & Sari 2002; Barniol Duran et al. 2013; Matsumoto & Piran 2023). Continuous monitoring of events in which early time ( $\sim$  days to weeks after the optical flare) radio emission was detected, like Swift J1644+57 (Zauderer et al. 2011) and ASASSN-14li (Alexander et al. 2016), demonstrated that the radio emission can be very long-lived, until  $\sim$  years after the disruption.

However, there are TDEs like ASASSN-15oi and AT2018hyz, in which early-time radio observations resulted in null detections, yet continued monitoring of these events until late time ( $\sim$  months to years after the optical flare) resulted in radio detections (Horesh et al. 2021; Cendes et al. 2022). This can be either due to a delay in the ejection of the outflow (Cendes et al. 2022) or due to the viewing effects of an off-axis observer looking at a relativistic jet (Matsumoto & Piran 2023; Sfaradi et al. 2024). In addition, Horesh et al. (2021) found a radio re-brightening in ASASSN-15oi,  $\sim 4$  years after the

initial optical discovery. Horesh et al. (2021) and Cendes et al. (2022) showed that the radio light curve in both these events showed a rise/decline that is steeper than any of the current predictions. More recently, studying late-time radio activity in TDEs using a sample of 23 TDEs, Cendes et al. (2023) showed that the launch of outflow can be delayed, by as much as  $\sim 700$  days, which raises the question of whether the phenomenon of delayed ejection is common in TDEs and whether the current models are adequate for describing the observed emission in TDEs like these.

While large samples of TDEs are coming from ongoing optical surveys (van Velzen et al. 2020; Gezari 2021; Yao et al. 2023), the discovery space is expanding. Recent studies like those of van Velzen et al. (2016, 2021); Jiang et al. (2021) and Masterson et al. (2024) have discovered TDEs at infrared (IR) wavelengths using dust echoes from TDEs. Using the first two epochs of the Very Large Array Sky Survey [VLASS; vllass, Somalwar et al. (2023) produced an independent sample of six radio TDEs that are optically bright. A few TDEs in this sample showed lower blackbody temperatures ( $T_{bb}$ ) and luminosities ( $L_{bb}$ ) compared to the optically discovered TDEs, indicating TDEs occurring in dust-obscured environments and adding to the sample of radio-first TDE discoveries (Anderson et al. 2020; Ravi et al. 2022). Such independent TDE discoveries from highly dust-obscured regions at radio/IR wavelengths can help constrain the true rate of TDEs and resolve the tension between the observed rate and the expected rate from theoretical predictions (Gezari 2021; Alexander et al. 2020; Yao et al. 2023). Using the first three years of data from the Zwicky Transient Facility (ZTF; Bellm et al. 2019), Yao et al. (2023) estimated a volumetric rate of  $3.1_{-1.0}^{+0.6} \times 10^{-7}$  Mpc<sup>-3</sup> yr<sup>-1</sup> TDEs ( $L_{bb} > 10^{43}$  erg/s). Comparing the rate of thermal TDEs to Swift J1644-like X-ray events (Alexander et al. 2020) and AT2020cmc-like optical events (Andreoni et al. 2022), the relative rate of jetted TDEs is estimated to be less than one percent of the thermal TDEs. This implies that the observed rate of thermal plus jetted TDEs is still lower than the current theoretical prediction by an order of magnitude (Gezari 2021).

All-sky radio surveys can be an extremely useful resource in discovering radio afterglows serendipitously. However, multi-epoch data can be crucial to separate emission related to the TDE to emission from any active galactic nucleus (AGN) which may be present. In particular, high cadence surveys like the Australian SKA Pathfinder Variable and Slow Transients survey (ASKAP VAST; Murphy et al. 2013, 2021), can be very

<sup>1</sup> This is true for sun-like stars. In general, the spectral signature depends on the composition of the disrupted star.

fruitful in getting a well-sampled light curve<sup>2</sup> for a larger sample of TDEs where dedicated follow-up of every individual event may not be possible/practical (see e.g., [Leung et al. 2023](#), for a serendipitous discovery of an off-axis TDE afterglow candidate). Motivated by this, we used the data from the Rapid ASKAP Continuum Survey (RACS; [McConnell et al. 2020](#); [Hale et al. 2021](#)), a multi-epoch all-sky survey (see [Table 1](#) for survey details) to search for radio emission from TDEs discovered at higher energies (O/UV/X-ray). We then studied the prospects of finding radio TDEs in the VAST survey by projecting the rates estimated from the fraction of TDEs that are radio bright in the RACS survey.

An alternate approach of discovering TDEs by modeling the radio light curve evolution using existing models (e.g., [Nakar & Piran 2011](#)) is used by [Dykaar et al. \(2024\)](#) to independently discover TDE candidates at radio wavelengths. Our approach is different from the untargeted and model-dependent search of [Dykaar et al. \(2024\)](#), yet complementary since we find afterglows from TDEs like ASASSN-15oi, AT2018hyz etc, in which the observed radio emission can not be easily explained by the existing models. Unlike dedicated follow-up campaigns that extensively monitor a given sample of TDEs ([Cendes et al. 2023](#); [Somalwar et al. 2023](#)), our approach is different, in that we study the prospects of discovering TDEs serendipitously in all-sky surveys, and hence our data are sparser. We focus instead on the nature of the TDEs we detect at lower observing frequencies, their rates, and the implications and expectations for the VAST survey.

Our article is structured as follows: in [Section §2](#), we detail our observations, surveys used in this study, and our data reduction methods. In [Section §2.4](#) we discuss our sample selection technique. We present our detections in [Section §3](#) and describe the properties of the individual candidates in [Sections §3.1](#) through [§3.6](#). Finally, we discuss the implications of our detections in [Section §4](#) and projections for future surveys like VAST in [Section §4.2](#), before concluding in [Section §5](#).

Throughout this work, we use the [Planck Collaboration et al. \(2020\)](#) model of cosmology, with  $H_0 = 67.4 \text{ km Mpc}^{-1} \text{ s}^{-1}$ .

## 2. OBSERVATIONS AND DATA ANALYSIS

### 2.1. Rapid ASKAP Continuum Survey (RACS)

The primary data set used in this work comes from all-sky 887.5 MHz radio observations taken as a part of

RACS — RACS-low. RACS-low has been conducted at two separate epochs thus far, separated by  $\sim 3$  years. In addition, RACS has also been conducted at two other frequencies, as single (so far) epoch surveys — RACS-mid (1367 MHz; [Duchesne et al. 2023](#)) and RACS-high (1655 MHz; *in prep.*), data from which we have used to study the behavior of the TDEs that we detected in RACS-low. Details of each of these surveys are provided in [Table 1](#).

Observations for all of the RACS surveys were carried out between March 2019 and April 2022. Data were processed using standard techniques recommended for ASKAP data ([Hotan et al. 2021](#)), using the ASKAPSOFT package ([Guzman et al. 2019](#)), to generate both the images and the noise maps. A more detailed description of reduction techniques is provided by [McConnell et al. \(2020\)](#). In this paper, we only used the total intensity (Stokes I) maps.

### 2.2. Variable and Slow Transients Survey (VAST)

VAST ([Murphy et al. 2013, 2021](#)) is a radio survey that will image almost one-quarter of the entire sky repeatedly for 4 years. VAST is divided between the Galactic and extra-galactic sky with the Galactic sky being observed with a cadence of roughly 2 weeks and the extra-galactic sky with a cadence of roughly 2 months. VAST pilot surveys ([Murphy et al. 2021](#)) were carried out in-between the two RACS-low epochs, and the main VAST survey<sup>3</sup> began its operation in December 2022. For the TDEs that we detected in the RACS-low dataset, we augmented the RACS data with data from the VAST survey, if the transient falls inside the VAST footprint. The survey parameters of VAST are similar to the RACS-low (see [Table 1](#)) survey, except for a 12 min integration time per field in VAST compared to a 15 min observation in RACS. A more detailed description of the pilot and the full surveys is provided by [Murphy et al. \(2013, 2021\)](#); [Leung et al. \(2023\)](#); [Pritchard et al. \(2024\)](#).

### 2.3. VLA Sky Survey (VLASS)

In addition to the RACS and VAST survey data, we also made use of the VLA Sky Survey (VLASS; [Lacy et al. 2020](#)). VLASS is an all-sky survey<sup>4</sup> spanning 2-4 GHz and plans to scan the entire sky at three different epochs with a cadence of roughly 32 months between the epochs. The first two epochs have been completed and the third epoch is underway. For the TDEs detected in

<sup>2</sup> VAST has a cadence of 2 weeks–2 months depending on the sky position.

<sup>3</sup> <https://www.vast-survey.org/Survey/>

<sup>4</sup> North of  $-40^\circ$  declination.

**Table 1.** Survey details of all the different surveys used as a part of this article.

Survey	RACS-low (epoch 1)	RACS-low (epoch 2)	RACS-mid	RACS-high	VLASS
Center frequency (MHz)	887.5	887.5	1367.5	1655.5	3000
Bandwidth (MHz)	288	288	144	200	2000
Sky coverage	$-90^\circ < \delta < +41^\circ$	$-90^\circ < \delta < +51^\circ$	$-90^\circ < \delta < +49^\circ$	$-90^\circ < \delta < +48^\circ$	$-40^\circ < \delta < +90^\circ$
Integration time	15 min	15 min	15 min	15 min	5 s
Median noise (mJy/beam)	0.25	0.19	0.20	0.19	0.12
Angular resolution	$\sim 15''$	$\sim 15''$	$\sim 10''$	$\sim 8''$	$2.5''$
Observations	$\sim$ March 2019	$\sim$ March 2022	$\sim$ January 2021	$\sim$ December 2021	... <sup>a</sup>
Instrument	ASKAP	ASKAP	ASKAP	ASKAP	VLA
Reference	McConnell et al. (2020)	in prep.	Duchesne et al. (2023)	in prep.	Lacy et al. (2020)

<sup>a</sup>The first two epochs of VLASS were completed roughly in 2019 and 2021, and the third observing run is currently ongoing.

RACS-low data, we used the VLASS quick-look images<sup>5</sup> (Lacy et al. 2020) to measure the flux density at 3 GHz.

#### 2.4. Search methodology

We selected all the TDEs from the transient network server (TNS)<sup>6</sup> that were spectroscopically classified as TDEs, as well as those that were optically discovered in all-sky surveys like the ZTF and All-Sky Automated Survey for Supernovae (ASAS-SN<sup>7</sup>; Shappee et al. 2014), which resulted in 63 events (Auchettl et al. 2017; Hammerstein et al. 2023; Yao et al. 2023). We then discarded 13 events that are outside the RACS-low epoch 1 footprint, as well as those events where the optical discovery occurred after RACS-low epoch 2, leaving 43 events in our sample. We examined the RACS-low total intensity (Stokes I) sky maps to look for radio emission at the TDE positions. Radio emission in TDEs can be observable  $\sim$ years after the initial disruption<sup>8</sup> (see Alexander et al. 2020; Cendes et al. 2022; Sfaradi et al. 2024; Cendes et al. 2023) and hence we restricted our cross-match to spatial coincidence, relaxing any constraint on the temporal coincidence as long as the TDE was discovered before the second RACS-low epoch. The positional accuracy for the ASKAP data is  $2.5''$ <sup>9</sup> and hence we used twice this as our search radius,  $5''$ , when astrometrically crossmatching the TDEs.

<sup>5</sup> <https://archive-new.nrao.edu/vlass/quicklook/>

<sup>6</sup> <https://www.wis-tns.org/>

<sup>7</sup> <https://www.astronomy.ohio-state.edu/asassn/>

<sup>8</sup> The radio emission can persist for  $\sim$  years after the optical flare (like Swift J1644; Zauderer et al. 2011) in a few TDEs, but is only observable at late times (like ASASSN-15oi; Horesh et al. 2021) in a few others.

<sup>9</sup> This is including the systematic component of the offset (see McConnell et al. 2020).

This resulted in 11 TDEs for which we detected coincident radio emission in RACS-low. However, only 5 of these events showed significant variability in their light curve between the two RACS-low epochs. The remaining 6 events did not show any significant evolution between the RACS-low epochs, which made it difficult to rule out underlying host galaxy/host AGN emission (see Section §3.6 for more details).

In the five TDEs with coincident variable radio emission, the emission lasted  $\sim$ years after the initial optical outburst, with the longest radio lived TDE lasting  $\sim 8$  yrs. Our detections add to the sample of TDEs reported by Cendes et al. (2023), where late-time radio emission is seen. However, only one TDE (AT2018hzy) is common between our sample and Cendes et al. (2023). Table 2 gives the flux density measurements for all these events. For all the TDEs that are in the RACS footprint, but resulted in non-detections we provide upper limits ( $3\text{-}\sigma$ ) on the radio flux density and radio luminosity in Table 3.

### 3. INDIVIDUAL TIDAL DISRUPTION EVENTS

Given the nature of this study, our light curves are sparser than dedicated campaigns like those of Goodwin et al. (2022b) or Cendes et al. (2022, 2023). We therefore make simplifying assumptions about the spectral and temporal properties of the observed emission to estimate the source properties. We modeled the late-time radio spectrum as a broken power-law with the break frequency corresponding to synchrotron self-absorption (SSA) frequency ( $\nu_{\text{ssa}}$ ), but adapted from Granot & Sari (2002) to join the power-laws smoothly (see case 2 of Figure 1 of Granot & Sari 2002). We modeled the temporal evolution of the light curve using Chevalier (1998): a rising power-law when the emission is optically thick

smoothly joined by a declining power-law when the emission becomes optically thin.

To infer source parameters we assume that the energy stored in magnetic fields is similar to the energy of the relativistic electrons, (*equipartition*; Pacholczyk 1970). Since the time scale of our radio detections is  $\approx$  year(s), unless we see evidence for on-axis jets (radio luminosity consistent with Swift J1644 or AT2020cmc-like events) or off-axis relativistic jets (characterized by steep rise time), we assume that the bulk Lorentz factor is close to 1 (Newtonian case). We assume that roughly 10% of the energy in heavy particles is used to accelerate the electrons to relativistic speeds ( $\epsilon_e \approx 0.1$ ). Assuming a power-law seed electron energy distribution  $N(E)dE = AE^{-p}$ , with  $p$  being the index, we infer the emission radius ( $R_{\text{eq}}$ ) and the total equipartition energy following Barniol Duran et al. (2013)<sup>10</sup>. We caution that the outflow geometry of sub/non-relativistic outflows can be quasi-spherical or asymmetrical, in which the filling factors can differ, but as noted by Pacholczyk (1970), the estimated source properties are relatively insensitive to these. Hence, in this work, we assume that the geometry is nearly spherical. Further, we assume that the observed radio emission arises from a thin shell of expanding outflow (of width  $\approx 0.1R$ , where  $R$  is the radius, e.g., Alexander et al. 2016) and is spherically symmetric. For such cases, the areal and volume filling factors,  $f_A$ , and  $f_V$  (see Barniol Duran et al. 2013) are 1 and 0.36 respectively.

### 3.1. ASASSN-15oi

After an initial non-detection at radio wavelengths (up to  $\sim 6$  months), Horesh et al. (2021) reported the discovery of a radio counterpart to ASASSN-15oi (Holoien et al. 2016) that rose steeply ( $\sim t^4$ ). This was followed by a steep fall (steeper than  $t^{-3}$ ) that became shallower at late times (see Figure 1). Horesh et al. (2021) noted that such steep rise and fall times could not be explained by a standard forward shock and CNM interaction model. Horesh et al. (2021) also reported a very late time re-brightening ( $\sim 1000$  days later) in the VLASS epoch 1 data.

We detected very late time re-brightening in RACS-low data and the lightcurve continued to rise (roughly as  $\sim t^2$ ) and peaked  $\sim 2500$  days after the optical flare (see Figure 1). This very late time re-brightening was replicated in the RACS-mid and RACS-high data as well. VAST observations for this transient revealed that the

emission started to decline steeply ( $\sim t^{-3}$ ) following the peak. This very late time decline is similar to the behavior that Horesh et al. (2021) reported following the initial radio peak. As Horesh et al. (2021) points out, the changes in various decline rates of emission could point to changes in the CNM density profile or a structured jet. However, it is difficult to reconcile such steep rise and fall times with the existing afterglow models.

Using the second epoch of VLASS observations, we find that the 3 GHz light curve is declining, roughly following a  $t^{-1}$  decline (see Figure 1). This is in contrast to the rising 887.5 MHz light curve during the same period, which suggests that the emission at 3 GHz was optically thin during this period and that at 887.5 MHz was optically thick. This can be explained by the peak frequency gradually transitioning to lower frequencies at late times, a trend that is expected and was also observed by Horesh et al. (2021) during the initial radio observations. This is also consistent with our 887.5 MHz observations, which revealed a turnover indicative of emission transitioning from optically thick to thin at  $> 3000$  days.

The RACS-high, VLASS epoch 2, and the RACS-low epoch 2 data are separated by  $\sim 75$  days, and under the assumption that the spectral evolution during this time frame is minimal (given the active cycle of  $> 4$  years), we found that the spectrum at this epoch ( $\sim 2400$  d after the event) is well fit by a power law (with the spectra index,  $\alpha = -0.75 \pm 0.2$ , where  $S_\nu \propto \nu^\alpha$ ). We assumed that the self-absorption frequency is closer to the RACS observing frequency (887.5 MHz)<sup>11</sup>, without attempting a physical model for the origin of this<sup>12</sup>, and estimate the electron distribution index  $p = 2.5 \pm 0.2$ . Given the peak frequency  $\nu_p \approx 887.5$  MHz, the peak flux density  $F_{\nu,p} = 12.2$  mJy, and  $p = 2.5$ , we derive a lower limit of  $R_{\text{eq}} \approx 6 \times 10^{17}$  cm, on the emission radius and  $E_{\text{eq}} \approx 1 \times 10^{50}$  erg on the total energy.

### 3.2. AT2019ahk / ASASSN-19bt

AT2019ahk was discovered as an optical transient by Holoien et al. (2019). We report an independent radio discovery of this event in RACS data at all three frequencies (see Figure 2), where we saw a rising transient over 3 years. Christy et al. (2024) reports archival radio detection of AT2019ahk roughly 4 years before the disruption and estimates underlying host galaxy emis-

<sup>10</sup> Since the peak frequency corresponds to  $\nu_{\text{ssa}}$ , we correct the total equipartition energy by accounting for the radiation emitted at  $\nu_m$ .

<sup>11</sup> The radio emission being optically thick at 887.5 MHz at this time (which continues until  $\sim 2800$  days after the disruption) and thin at 3 GHz partially supports this assumption.

<sup>12</sup> Horesh et al. (2021) found that the initial radio spectrum showed large deviation from the SSA spectrum in the self-absorbed part, but might be consistent with free-free absorption.

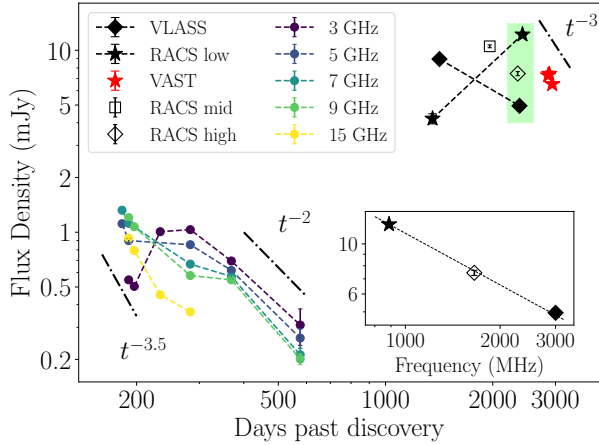


**Figure 1.** Lightcurve of the TDE ASASSN-15oi using RACS, VLASS, and archival data. In all the figures in this article, RACS-low data is shown as black stars, RACS-mid as open black squares, RACS-high as open black diamonds, and VLASS data as filled black diamonds. RACS data combined with the data from the VAST full survey, shown as red stars, reveal the rise and decline of the 888 MHz light curve. Shown as multicolored dots is the archival lightcurve, from 3 GHz to 15 GHz, adapted from Horesh et al. (2021). The green stripe shows the data used to estimate the electron distribution index. The inset plot shows this spectrum and the dashed line in the inset plot shows the best-fit power law to these data (see text for more details). Shown as dashed-dotted lines are the visual guides for different power-law declines.

sion to follow  $F_{\nu, \text{host}} = 0.439 (\nu/2.1)^{-1}$  mJy. Combining the RACS data with contemporaneous data from Christy et al. (2024), we see that the 0.8–0.9 GHz light curve is still rising  $\approx 1500$  days after the event, but the 1.6 GHz light curve started to decline. This hints that emission at 1.6 GHz has transitioned to an optically thin regime, but emission at lower frequencies is still optically thick. Hence, the SSA frequency is very close to RACS-high the frequency at  $\approx 1100$  days, consistent with the peak frequency estimated by Christy et al. (2024). Using  $p \approx 2.7$  (using existing literature, e.g., Goodwin et al. 2022b; Cendes et al. 2022, 2023 and also consistent with Christy et al. 2024), we estimate the equipartition emission radius for  $\nu_p = 1.655$  GHz,  $F_{\nu, p} = 6.4$  mJy to be  $\approx 1 \times 10^{17}$  cm and total energy to be  $\approx 7 \times 10^{48}$  erg at  $\delta t = 1100$  days.

### 3.3. AT2019azh

Using multi-frequency observations of multiple epochs, Goodwin et al. (2022b) modeled the radio spectrum of AT2019azh to find a free expansion of the ejecta that showed signs of deceleration post  $\sim 450$  days of the disruption. Sfaradi et al. (2022), on the other hand, modeled the 15.5 GHz lightcurve and found evidence for two emission components (see Figure 3), which led the

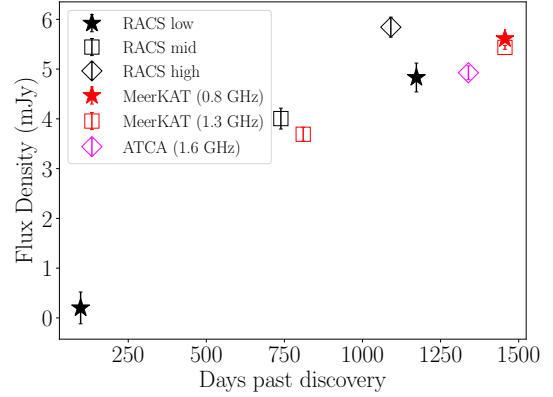


**Figure 2.** Lightcurve of the TDE AT 2019ahk confirming the late-time rise of radio light curve at all the RACS observing frequencies. Also shown are the contemporary data at 1.3 GHz and 1.6 GHz adapted from Christy et al. (2024) showing the continued rise of 0.8–0.9 GHz light curve, turn over of 1.6 GHz light curve. This source is too far south for VLASS.

authors to propose a state transition similar to the ones observed in X-ray binaries.

We found this TDE in the RACS-low data as a slowly rising source, increasing by a factor of  $\sim 2$  between the two epochs. We also detected this source in the RACS-mid and RACS-high data sets. Using the RACS-mid data and the data from Goodwin et al. (2022b), we modeled the 1.4 GHz lightcurve reasonably well by a two-component model similar to Sfaradi et al. (2022). Figure 3 shows the full light curve for this event where the similarity can be seen between the shapes of the 15.5 GHz and 1.4 GHz light curves, although the rise and fall times at these frequencies are different. At 1.4 GHz, the two components rose to a peak at  $\sim 300$  and 520 days respectively, slower than the 15.5 GHz light curve that took 130 days and 360 to rise. This is broadly consistent with the underlying model Chevalier (1998) where the emission at different frequencies is self-similar but the emission at lower frequencies has longer rise times.

However, the very late time ( $\gtrsim 3$  yrs) relative behavior between the RACS-mid and the RACS-high data is puzzling. Goodwin et al. (2022b) noted that the peak frequency at late times was  $< 1$  GHz, which meant that the spectrum above this should be a declining one. But the observed flux density in RACS-high is higher than the model-predicted flux density in RACS-mid by a factor that is roughly consistent with the SSA mechanism (where  $S_\nu \propto \nu^{5/2}$ ). This might be indicative of the peak frequency increasing to higher frequencies at late times, something that Cendes et al. (2022) observed in another event, AT2018hyz, indicative of late-time source activity. The RACS-low second epoch detection postdates

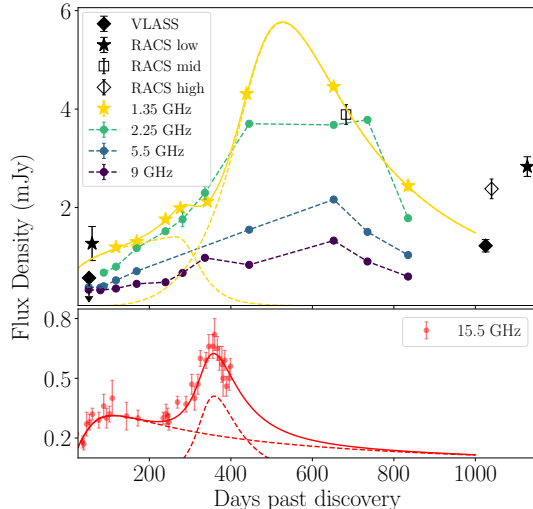


**Figure 3.** *Top panel:* The light curve using archival data (from Sfaradi et al. 2022; Goodwin et al. 2022b) is shown at 4 different frequencies (1.3, 2.25, 5.5, 9 GHz). The yellow curve is the best-fit model for the 1.4 GHz data (see text for the model), with the dashed lines representing the individual components and the solid line indicating their sum. *Bottom panel:* 15.5 GHz lightcurve for reference using the data from Sfaradi et al. (2022). The red curve is the two-component model proposed by Sfaradi et al. (2022), with the dashed line representing the individual components and the solid line, their sum.

this, however the lack of continued coverage through very late times makes it difficult to distinguish whether this consistent with the initial decline, or is a signature of very late time rebrightening, as hinted by the RACS-high data.

The RACS-high and VLASS observations are separated by  $\approx 14$  days; under the assumptions that i) this interval is much shorter than the evolutionary timescale of the radio emission, and ii) the peak frequency rose, but to a value lower than the observing frequency of RACS-high. We estimated the electron distribution index to be  $p = 3.2 \pm 0.4$  (at  $\Delta t = 1030$  days), consistent with the electron distribution of Goodwin et al. (2022b) at late times (849 days). This seems to hint that the emission we see at very late times might still be coming from the same family of electrons.

### 3.4. AT2018hyz

AT2018hyz was first detected at radio wavelengths  $\sim 2.5$  years after the optical outburst (Horesh et al. 2022), and showed an unusually steep rise ( $\sim t^{4-6}$ ) at most of the observed frequencies (1.3-19 GHz) (Cendes et al. 2022; Sfaradi et al. 2024). Cendes et al. (2022) noted that the light curve at lower frequencies ( $\lesssim 3$  GHz) began to decline (see Figure 4) at the end of their observ-

ing campaign ( $\sim 1250$  d past optical outburst). Modeling the spectrum at multiple epochs, Cendes et al. (2022) also found that the peak frequency increased roughly from 1.5 GHz to 3 GHz at late times. However, following the off-axis jet model proposed by Matsumoto & Piran (2023), Sfaradi et al. (2024) showed that the observed radio emission in AT2018hyz is also consistent with late-time emission from a narrow jet ( $\sim 7^\circ$ ) as viewed by an off-axis observer ( $\sim 42^\circ$ ).

Upon finding this source in RACS-low data, we looked at the detailed VAST light curve and found no discernible radio emission until late times and a very steep rise at late times ( $\sim t^4$  rise; see Figure 4), both of which were consistent with Cendes et al. (2022) and Sfaradi et al. (2024). We also found that the 887.5 MHz emission continued to rise until our final observation ( $\Delta t = 1700$  days)<sup>13</sup>. However, given the steep rise of this particular transient and the gap between RACS-low epoch 2 and the VAST full survey data, we cannot rule out a decline seen by Cendes et al. (2022) at frequencies below 3 GHz, followed by a rebrightening at 887.5 MHz instead of a single brightening episode.

We then investigated the sudden jump in the peak frequency from 1.5 GHz to 3 GHz reported by Cendes et al. (2022) (see Figure 3 and Section 4.1 of Cendes et al. 2022). At day 1251, Cendes et al. (2022) found that the peak frequency is 1.5 GHz but the data used in this fit were all at frequencies  $> 1.12$  GHz, where the self-absorbed part of the spectrum might not have been well captured. Combining the 887.5 MHz RACS data from day 1263 with the data from day 1251, we found that the peak frequency rose to 1.9 GHz, as opposed to 1.5 GHz. At this epoch, we also find that the absorption part of the spectrum is more or less consistent ( $S_\nu \sim \nu^{2.7}$ ) with what is expected from the SSA mechanism ( $S_\nu \propto \nu^{5/2}$ ). This rise in the peak frequency to roughly 3 GHz at day 1282 might be explained by this gradual increase in the peak frequency rather than a sudden shift, something similar to what we found in AT2019azh (see §3.3).

Using the latest epoch of VLASS data, we found that the 3 GHz emission also rose from an early non-detection as  $t^4$  (see Figure 4), consistent with the RACS/VAST data, to a remarkably bright 16.5 mJy. This is consistent with the very late-time brightening of this transient in radio.

### 3.5. AT2019qiz

<sup>13</sup> Using the data from our latest observation at 1757 days, we find a hint of a turn-over in the 887.5 MHz lightcurve, but we need additional data to robustly confirm this.

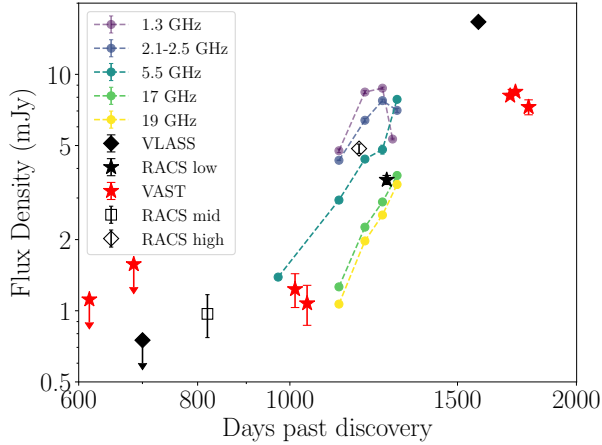


**Figure 4.** Light curve of TDE AT2018hyz using RACS/VAST data, VLASS data, and archival data (from Cendes et al. 2022). The archival lightcurve, at 5 different frequencies from 1.3 GHz to 19 GHz, adapted from Cendes et al. (2022), is shown as multi-colored dots for reference.

AT2019qiz (Siebert et al. 2019; Nicholl et al. 2020; Hung et al. 2021; Patra et al. 2022) has received comparatively very little follow-up at radio wavelengths, with O’Brien et al. (2019a,b) presenting the initial radio detections that indicated a rising transient at multiple frequencies but with no robust analysis presented (see Figure 5).

We found this transient in RACS-low data brightening from a non-detection in epoch 1 to a flux density level of  $\sim 1$  mJy in the second epoch of RACS-low, consistent with RACS-mid and RACS-high. This suggests that this source might be very slowly evolving or that it may be steadily emitting at higher flux density levels. The VAST full survey data resulted in a non-detection, which indicated that the flux density variation was  $<30\%$  of the mean (see Figure 5). We also inspected the VLASS epoch 1 image that predated the optical disruption time and did not find a detection putting a  $3\sigma$  upper limit of 0.36 mJy on the persistent emission at 3 GHz. However, the transient rose to persistent levels of 1 mJy in the latter VLASS epochs (see Figure 5).

Motivated by this behavior, we wanted to see if the early-time behavior was consistent with an afterglow or if it was different, in which case it might provide clues to the nature of the underlying emission. Using the data from O’Brien et al. (2019a,b), we found that the initial rise time estimated at different frequencies seems to be consistent with  $t^{2.5}$  at both 17 and 9 GHz. This  $t^{2.5}$  increase was also consistent with the non-detection of this transient at 5.5 GHz at early times. The spectrum at  $\sim 75$  d seemed to be inconsistent with a synchrotron self-absorption spectrum ( $S_\nu \propto \nu^{5/2}$ ), so, we tried to

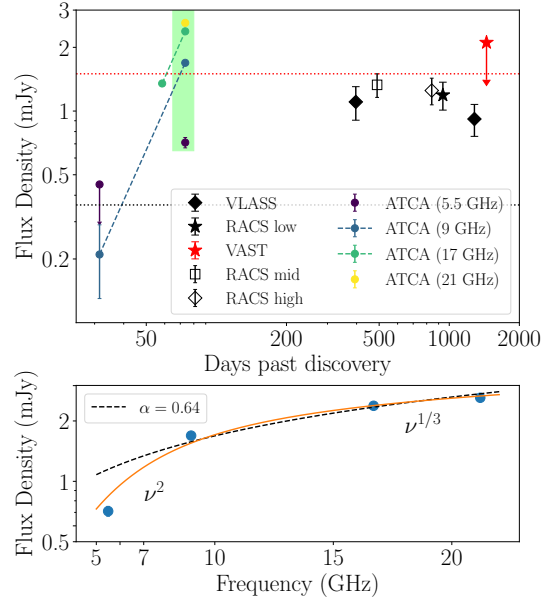


**Figure 5.** *Top panel:* Light curve of the TDE AT2019qiz using RACS, VLASS, and archival data at 4 different frequencies from 5.5 GHz to 21 GHz from O’Brien et al. (2019a,b). The green stripe shows the multi-frequency epoch at  $\sim 75$  d which we use for spectral fitting. The black dotted line shows the  $3\text{-}\sigma$  pre-disruption limit from VLASS data and the red dotted line shows the same from RACS-low epoch 1 data. *Bottom panel:* Spectrum of this transient using observations at 4 different frequencies taken at the same epoch ( $\sim 75$  d post optical discovery; indicated by the box in the top panel). The orange line is the best fit broken power-law to the observed spectrum (see section §3.5). The dashed black line is the best fit single power-law spectrum (with spectral index  $\alpha = 0.64$ ).

model the break frequency as minimal frequency ( $\nu_m$ ) instead of self-absorption frequency (see spectrum 1 in Figure 1 of Granot & Sari 2002). Here the two rising power-laws spectral indices are  $+2$  (Rayleigh-Jeans tail) at frequencies below the break and  $+1/3$  at frequencies above the break frequency. We found a reasonable fit to the spectrum in this case (see bottom panel of Figure 5) with the break frequency around  $\sim 9$  GHz. This is indicative that at early times the emission seems to be consistent with an afterglow.

We tried to reconcile with the late-time radio observations from RACS and VLASS. The lack of late-time evolution likely ruled out the scenario where the late-time activity was still dominated by the emission powered by the CNM interaction. It is also possible that there was prior nuclear activity (possibly from an AGN) in this galaxy which is visible once the transient faded away. The non-detection in VLASS and RACS data before



the optical discovery makes this unlikely<sup>14</sup>, but cannot be ruled out entirely. Although not temporally simultaneous, if we assume that the source is persistent and non-variable, the spectrum might be consistent with a flat spectrum at late times, using the RACS and VLASS data. It might be possible that a jet was launched at early times and we are looking directly into the emission from the jet at late times, which could explain the flat spectrum. If this were the case, then it might be an interesting situation in which late-time emission from the jet was directly seen and would add to the small sample of jetted radio TDEs, but given the sparsity of the data, it cannot be firmly established.

### 3.6. Steady Radio Sources: Probable AGN/Host Galaxy Emission

In addition to the candidates where a rising/declining behavior is clearly seen, there are cases where the light curve showed little variation or was consistent with a non-varying source (the underlying host galaxy or AGN). An AGN may be intrinsically variable, or variable due to external effects like scintillation (Jauncey et al. 2016). In both cases, if the flux density was consistent with a steady source within error bars between the two RACS epochs, we considered that to result from underlying AGN activity (clearly this is a conservative assumption, as we could be averaging over peaks or declines given our sparse sampling). Below we note such examples (see Figure 6). We cross-matched the TDEs in our sample with the WISE catalog (Wright et al. 2010) to look for AGN signature. Figure 7 shows the identified counterparts on a WISE color-color plot (Wright et al. 2010). We used a color difference of  $WISE\ band\ 1\ (3.4\ \mu m) - WISE\ band\ 2\ (4.6\ \mu m) > 0.8$  (Wright et al. 2010) to classify an object as an AGN.

- **AT2020nov** was detected in both epochs of RACS-low with no significant evolution between them, and also in RACS-mid and RACS-high (see Figure 8). The first RACS-low observation predated the optical outburst by  $\sim 400$  days. We looked at the VLASS images and found that the same behavior was replicated at 3 GHz. Recently, Cendes et al. (2023) also reported AT2020nov as probably dominated by an AGN in their study, with a non-evolving light curve at 6 GHz. The lack of variability in the observed data seems to indicate that the radio emission is likely coming

from the AGN activity itself. Exploiting the non-variability of this at different frequencies, we estimated the spectral index (see Figure 8), assuming a power-law spectrum  $S_\nu \propto \nu^{-\alpha}$  for AGN activity. Using the data from RACS, VLASS and Cendes et al. (2023) to find  $\alpha = -0.64 \pm 0.04$ , consistent with the typical AGN spectrum (Condon et al. 2002; Sabater et al. 2019).

- **AT 2022dsb** was discovered by Stanek & Kochanek (2022) on 2022 March 01 and had a radio detection reported by Goodwin et al. (2022a) roughly 20 days later, but the transient nature of this source was not confirmed. RACS-low epoch 1 had a  $4\sigma$  pre-discovery measurement which points to an underlying AGN<sup>15</sup> or host galaxy emission, a conclusion strengthened by the detection in epoch 2 which showed little variability roughly 60 days after the optical outburst. There was also a pre-discovery measurement in RACS-mid. RACS-high and VLASS data resulted in upper limits ( $3\sigma$ ; 0.6 mJy and 0.36 mJy respectively). Based on these detections and upper limits, we estimated the spectral index to be  $\alpha = -0.7 \pm 0.3$ , typical of AGN.
- **AT 2022bdw** (Tonry et al. 2022): No radio detection from this source has been reported so far, but we found pre-discovery detections in RACS-low epoch 1 and RACS-mid data. Comparing it with RACS-low epoch 2, which was post optical outburst, we found that the flux density level was consistent with a non-varying source, either the host AGN or host galaxy emission<sup>16</sup>. No emission was found in RACS-high or VLASS data and using these we estimate the spectral index of the background emission to be  $\alpha = -0.8 \pm 0.3$ , again typical of AGN.
- **AT 2021qyv**: AT 2021qyv (Jones et al. 2021) was observed as a part of the VAST survey in addition to the RACS survey. However, no strong detection has been found in any of the RACS/VAST data except for detection in RACS-low epoch 2. RACS-mid showed a weak  $3\sigma$  detection at this location, with RACS-high, VLASS and FIRST data resulting in null detections, and hence we conclude

<sup>14</sup> In particular, the AGN flux density variation with respect to the VLASS non-detection in epoch 1 has to be at least a factor of  $\sim 5 - 6$ .

<sup>15</sup> There is a WISE counterpart within  $1''$  of this position, but the WISE colors were not sufficiently conclusive to claim an AGN.

<sup>16</sup> This was one of the few fields that was observed twice as a part of RACS-low epoch 2, separated by 45 days, and the flux density was consistent with a non-varying source to within  $2\sigma$ .

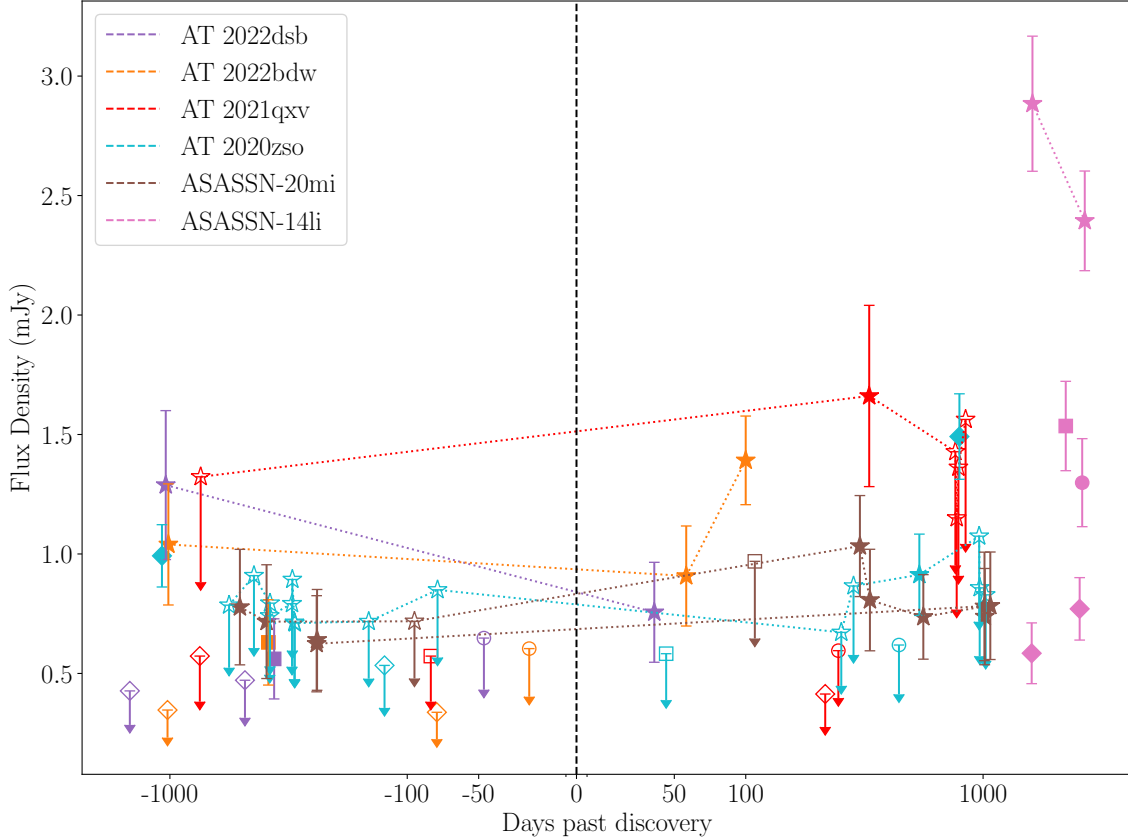


**Figure 6.** Lightcurves of the TDEs which did not show clear variability over the span of the RACS observations (roughly 3 yrs) and might be contaminated by host emission: AT 2022dsb (purple), AT 2022bdw (orange), AT 2021q xv (red), AT 2020zso (cyan), ASASSN-20mi (brown) and ASASSN-14li (magenta). For each TDE the RACS-low data are shown as stars, RACS-mid data as squares, RACS-high data as circles, and the VLASS data as diamonds. Filled markers represent detections and open markers represent upper limits. The black dashed line shows the optical outburst time. Where possible, we use RACS+VLASS measurements to estimate the spectral slope of the power law spectrum (see Section 3.6).

that the RACS-low epoch 2 detection that we see is probably coming from an underlying AGN<sup>17</sup> with a spectral index steeper than  $\alpha = -1.1$ .

- **AT 2020zso:** Discovered by Forster et al. (2020), very weak radio detection of  $22 \pm 7 \mu\text{Jy}$  at 15 GHz was reported roughly 1 month later by Alexander et al. (2021), but following this, a null detection was made with the uGMRT (Roy et al. 2021) at the central frequencies of 0.65 and 1.26 GHz (upper limits of  $46.6 \mu\text{Jy}$  and  $51.2 \mu\text{Jy}$ ). No strong detections were made in RACS/VAST data except for a single detection in RACS-low epoch 2. VLASS data contains a  $5\sigma$  detection in epoch 3.1, but the VAST observation that succeeded this resulted in non-detections so we cannot conclusively establish any late time transient activity from this source. It might be possible that

the transient might take longer to rise at lower frequencies (Chevalier 1998) in which case future data from the VAST full survey will be very useful to check this. However, with the current data, we cannot rule out AGN variability.

- **ASASSN-14li:** ASASSN-14li (Jose et al. 2014; Holoien et al. 2016; Alexander et al. 2016) showed late-time fading that continued until  $\sim 600$  days in some bands (Bright et al. 2018). We found radio detections at this position in both RACS-low epochs, but consistent with a steady flux density level. This source was also detected in RACS-mid, RACS-high, and VLASS, with no sign of evolution in the latter. Comparing the archival FIRST measurement  $2.68 \pm 0.15 \text{ mJy}$  at 1.4 GHz with the RACS-mid observations indicate a  $\sim 40\%$  decrease in the flux density, indicating that the transient possibly faded away and we are looking at the vari-

<sup>17</sup> WISE colors point to a probable AGN.

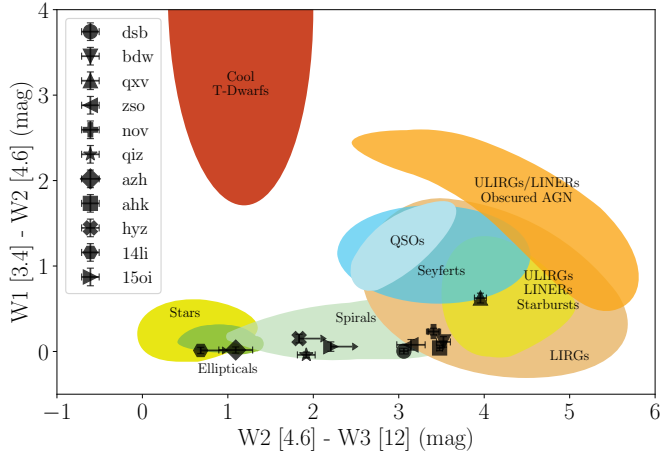


**Figure 7.** WISE color-color plot showing the magnitude difference in band 1 (W1) and band 2 (W2) on the Y axis, and band 2 (W2) and band 3 (W3) on the X axis. The contours for different object classes are adopted from Wright et al. (2010). We used a W1-W2 color of  $> 0.8$  to classify an object as AGN.

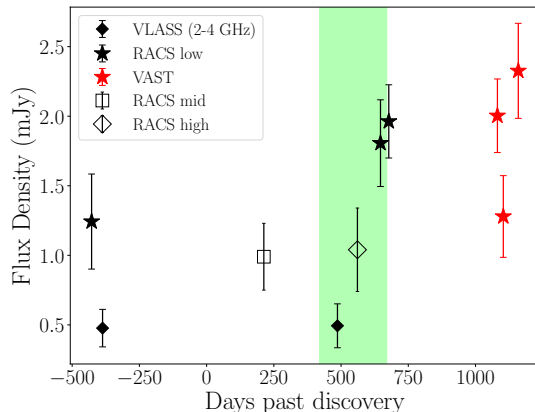


**Figure 8.** Light curve of TDE AT2020nov using RACS, VAST, and VLASS data, all resulting in detections, with very little variability. The green stripe shows the data points used to measure the spectral index of the power-law spectrum.

ability from an AGN. Using RACS, and VLASS data, we find the spectral index  $\alpha = -0.95 \pm 0.14$ .

## 4. DISCUSSION

### 4.1. On the nature of detections

Understanding the sample biases in all-sky searches is important in estimating the rates and expectations for future surveys. In particular, understanding if our radio-detected sample of TDEs forms an unbiased representation of the underlying optical population becomes important for future projections. Figure 9 shows the op-

tical properties of the TDEs (blackbody luminosity vs temperature, as estimated from the optical data) that resulted in radio detections in the RACS-low survey. Comparing the radio detections in optically discovered TDEs using the sample for this study and from Cendes et al. (2023), we do not see preferential occupation of radio-detected TDEs in this phase space. We do see that there are no radio detections of TDEs with both high temperatures and luminosities (top right corner of the plot), but that can be attributed to the redshift because we do not expect detectable radio emission<sup>18</sup> (given the current sensitivity limits of surveys like RACS/VLASS) from that sub-population. In the sub-sample of optical TDEs from which radio emission can be detected ( $z \lesssim 0.1$ ), our sample, as well as the sample from Cendes et al. (2023), is not biased towards certain classes of optical TDEs which suggests that the late-time detection of radio emission in TDEs might not be coming from a particular population of TDEs, but is a common feature of sub-relativistic TDEs in general. We then compare our estimates of the emission radius and minimum energy injected into the outflow with archival studies, under the equipartition situation (see Figure 10). We caution the reader that a strict comparison would need accurate modeling of the outflow expansion properties (linear/accelerating/decelerating) to compare estimates from different times. We hence restrict the sample to those that show late-time radio emission. Using the sample from Horesh et al. (2021); Cendes et al. (2022, 2023) and Christy et al. (2024), we find that our estimates for the emission radius and the energy injected are consistent with those reported in the literature.

Somalwar et al. (2023) did an untargeted search for TDEs using the first two epochs of VLASS data, and independently discovered radio-first detections of optically bright TDEs. These are shown as the green scatter in Figure 9. While some of these seem to be consistent with the population of optically selected radio TDEs, Somalwar et al. (2023) suggests that some radio-discovered optically bright TDEs can have lower black body temperatures and luminosities which partly can be due to TDEs occurring in dusty environments. Data from the RACS survey, but also more importantly from the VAST survey, which has a cadence of  $\sim 2$  months, should be very useful in conducting such untargeted searches.

### 4.2. Projections for the VAST survey

One of the important questions for an all-sky survey like RACS is the detection efficiency. Figure 11

<sup>18</sup> This is under the expectation of detecting radio emission from a sub-relativistic outflow with  $\nu L_\nu \approx 10^{38}$  erg/s.

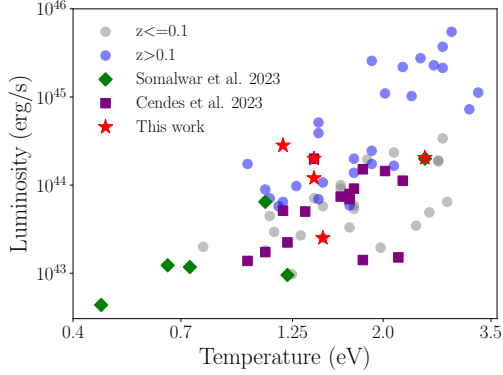


**Figure 9.** Blackbody luminosity vs temperature of the non-relativistic TDEs detected by various surveys. The background gray circles show the optical sample from the ZTF (Hammerstein et al. 2023; Yao et al. 2023) that are within a redshift of  $z=0.1$  and the blue circles show the TDE sample with  $z>0.1$ . The red stars show the optically-discovered TDEs that are detected in our radio sample. The purple squares show the optically discovered TDEs that resulted in radio detections in a targeted follow-up study by Cendes et al. (2023). The green diamonds show the TDEs that are independently identified in radio by Somalwar et al. (2023), but then confirmed optically. Where multiple points overlap, sources are common to multiple samples.

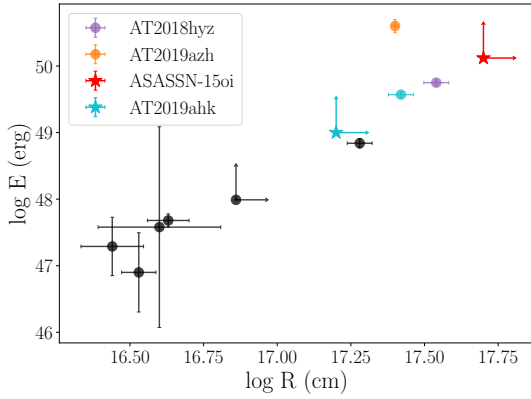


**Figure 10.** Estimates of equipartition radius and minimum total energy of the system, where possible, for the TDEs in our sample and archival TDEs (taken from Cendes et al. 2023). For our sample of TDEs, estimates derived from this study are shown as stars and those from the archival studies (Horesh et al. 2021; Cendes et al. 2022; Christy et al. 2024) are shown as circles. Estimates for archival TDEs that show late-time activity are shown as black dots (adapted from Cendes et al. 2023).

shows the radio luminosity at 887.5 MHz of the TDEs detected in the RACS survey compared to those of the population. We see that all of these detections have  $\nu L_\nu \approx 10^{38}$  erg/s. We caution that comparison between light curves from our sample at 887.5 MHz and archival

light curves at 6 GHz can be non-trivial and that the inferred radio luminosity  $\nu L_\nu$  can have frequency dependence if  $L_\nu$  does not exactly scale as  $\nu^{-1}$ . Thus, if the spectral index is steeper than  $-1$ , the radio luminosity, estimated from RACS will be an overestimation to the population (in Figure 11) and if shallower than  $-1$ , will be an underestimation. Despite this, if we assume  $\nu L_\nu \approx 10^{38}$  erg/s to be a typical estimate at 887.5 MHz, then given the sensitivity of RACS survey (RMS noise of 0.25 mJy/beam), then the survey should be complete out to  $z = 0.075$  ( $d_L = 350$  Mpc).

We then look at the total population of potentially detectable TDEs. We require that they i) are in the RACS footprint ( $< 41^\circ$  declination), ii) occurred before the RACS-low epoch 2 (April 2022), and iii) are within  $z = 0.075$ , which results in 23 TDEs. Out of these, we detect 5 candidates where we are most likely seeing the afterglow and as many as 6 other events where we might be seeing the host AGN. Counting the 5 detections yields a (90% confidence; estimated using Gehrels 1986) detection rate of  $22^{+15}_{-11}\%$ . This is slightly more than but consistent within errors with Alexander et al. (2020), but slightly less than Cendes et al. (2023), who finds late time radio activity in as much as 40% of optically selected TDEs. It is worth mentioning here that, unlike a targeted search (e.g., Cendes et al. 2023), where continuous monitoring is done after initial detection, our results are based on observations roughly separated by 3 yrs and hence we are completely insensitive to TDEs that rose and declined within this period, or to some of the most recent TDEs (that happened within a year of RACS-low epoch 2), which are still rising, but are currently below our sensitivity threshold. Hence this detection efficiency can be considered as a conservative lower limit for future efforts: a survey with a longer duration and finer time sampling would be able to detect more sources at the same sensitivity threshold.

Recently Cendes et al. (2023) performed a comprehensive late-time follow-up of a sample of 23 TDEs and found radio emission lasting on timescales of  $\sim$  a year in roughly 50% of the TDEs. Using the first three years of optical data from ZTF, Yao et al. (2023) constrained the volumetric rate of optical TDEs to be  $3.1^{+0.6}_{-1.0} \times 10^{-7}$  Mpc $^{-3}$  yr $^{-1}$ . If we assume that as many as 50% of optical TDEs (following Cendes et al. 2023) are capable of producing detectable late-time radio emission, then the current constraints on the rate of optical TDEs imply a rate of  $1.5 \times 10^{-7}$  Mpc $^{-3}$  yr $^{-1}$  for optically-selected, radio-emitting TDEs. This rate, coupled with the sensitivity of the VAST survey (RMS noise of 0.25 mJy/beam), its footprint (roughly a quarter of the total sky), and the survey lifetime (4 yrs),

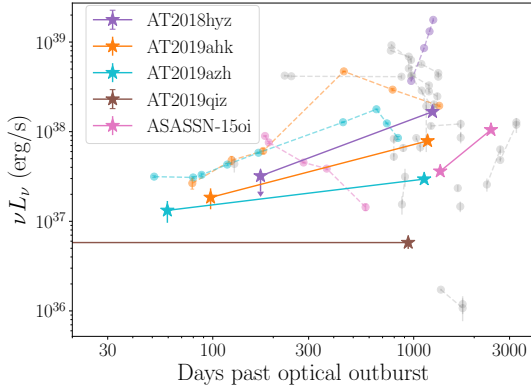


**Figure 11.** The radio luminosity of the 5 strong TDE detections in the RACS dataset at 887.5 MHz. The solid line shows radio luminosity from RACS detections while the dashed lines show the from same 5-7 GHz (data adapted from Horesh et al. 2021; Cendes et al. 2022; Goodwin et al. 2022b; Christy et al. 2024). Shown in gray in the background are the light curves (at 6 GHz) of the archival TDEs detected by Cendes et al. (2023) and Alexander et al. (2020) from optically selected TDEs.

implies that VAST should be able to detect  $\sim 20$  optically selected radio TDEs over the full survey. TDEs can also occur in highly dust-obscured environments, in which emission can be better studied at lower frequencies like the infrared where the emission can be powered by dust echoes (van Velzen et al. 2016; Jiang et al. 2021; van Velzen et al. 2021) and at radio wavelengths, that need ambient material for the outflows/jets to interact with. The rate of the radio-bright optically-quiet TDEs is highly uncertain currently, particularly due to the lack of such studies. Hence the above-mentioned sample of  $\sim 20$  TDEs can only be considered a lower limit on the detectable sample, given the current optical rate.

#### 4.3. RACS/VAST as a sub-GHz reference map

Radio emission from TDEs can last  $\sim$  years, and hence obtaining a robust host spectrum in the absence of one might imply that we need to wait for years before the transient fades away and the host galaxy dominates again. RACS, and in particular VAST, can be tremendously helpful in this respect since it provides a low-frequency (where the emission is brighter) reference image, that can be used to study the long-term variability (or lack thereof) of the host galaxy pre-explosion. To illustrate this, we provide the example of AT 2023clx where we can look for the pre-explosion radio emission using RACS data.

AT 2023clx was discovered by Stanek (2023) on 2023 February 22, well after RACS-low epoch 2. A radio detection was reported 4 days later by Sfaradi et al. (2023) consistent with the position of the optical tran-

sient. We found a persistent source in both epochs of RACS-low data at the optical location and, using non-detections in VLASS, we constrain the radio spectrum of the host to be steeper than  $-1.35$ . For future observing campaigns that aim to do dedicated follow-up of these TDEs, RACS data can be very useful in estimating the level of host contamination. With the availability of VAST full survey data, not only radio first discoveries can be made, but also a well-sampled light curve with a cadence of 2 months leading up to the optical outburst, can be obtained.

## 5. CONCLUSIONS

We conducted an untargeted search for radio emission in optically selected TDEs using data from the RACS survey, which resulted in 5 TDEs where the light curve showed significant evolution. For each of these TDEs, we modeled the evolution to show that the radio evolution at late times can undergo rebrightening and can be complex. We found that late-time activity can be quite common at radio wavelengths in sub-relativistic TDEs, adding to the sample presented by Cendes et al. (2023) who reached similar conclusions from targeted searches. Our search was based on the variability of the source over a timescale of roughly 3 years, which makes us insensitive to TDEs that evolve on timescales smaller than this, and we estimate the rate of optical TDEs in which late-time radio emission can be observed to be  $22^{+15}_{-11}\%$ . Using the current optical rates, we estimate a conservative lower limit on the number of TDEs that can be detected in the VAST survey to be  $\sim 20$  over its survey span (4 years).

1 We thank an anonymous referee for helpful comments.  
2 AA and DLK are supported by NSF grant AST-1816492.  
3 Parts of this research were conducted by the Aus-  
4 tralian Research Council Centre of Excellence for Grav-  
5 itational Wave Discovery (OzGrav), project number  
6 CE170100004. The Dunlap Institute is funded through  
7 an endowment established by the David Dunlap family  
8 and the University of Toronto. AH is grateful for the  
9 support by the the United States-Israel Binational Sci-  
10 ence Foundation (BSF grant 2020203) and by the Sir  
11 Zelman Cowen Universities Fund. This research was  
12 supported by the Israel Science Foundation (grant No.  
13 1679/23). HD acknowledges support from the Wal-  
14 ter C. Sumner Memorial Fellowship and the Natural  
15 Sciences and Engineering Research Council of Canada  
16 (NSERC) through a Postgraduate Scholarship. JP is  
17 supported by Australian Government Research Training  
18 Program Scholarships. KR thanks the LSST-DA Data  
19 Science Fellowship Program, which is funded by LSST-  
20 DA, the Brinson Foundation, and the Moore Foun-  
21 dation; Their participation in the program has bene-  
22 fited this work. GRS is supported by NSERC Dis-  
23 covery Grant RGPIN-2021-0400. This scientific work  
24 uses data obtained from Inyarrimanha Ilgari Bundara  
25 / the Murchison Radio-astronomy Observatory. The  
26 Australian SKA Pathfinder is part of the Australia  
27 Telescope National Facility (<https://ror.org/05qajvd42>)  
28 which is managed by CSIRO. Operation of ASKAP  
29 is funded by the Australian Government with support  
30 from the National Collaborative Research Infrastructure  
31 Strategy. ASKAP uses the resources of the Pawsey Su-  
32 percomputing Centre. The establishment of ASKAP,  
33 the Murchison Radio-astronomy Observatory, and the  
34 Pawsey Supercomputing Centre are initiatives of the  
35 Australian Government, with support from the Govern-  
36 ment of Western Australia and the Science and Industry  
37 Endowment Fund.

**Table 2.** Radio properties of the TDEs found in RACS-low data set.

Name	RA	DEC	Discovery (UT)	z	$\delta t$ (days)	RACS low (mJy)	RACS mid (mJy)	RACS high (mJy)	VLA55 (mJy)
ASASSN-15oi	2015-08-14	20h39m09.1s	-30d45m21s	0.02	1355.1	4.21 $\pm$ 0.27	...	...	...
					1417.3	...	...	8.95 $\pm$ 1.35	
					1961.3	...	10.52 $\pm$ 0.19	...	
					2350.2	...	...	7.45 $\pm$ 0.2	
					2377.7	...	...	...	4.95 $\pm$ 0.76
					2424.0	12.2 $\pm$ 0.15	...	...	
					2860.9	7.28 $\pm$ 0.17	...	...	
AT2019ahk	2019-01-29T21:50:24	07h00m11.5s	-66d02m24s	0.026	97.5	1.24 $\pm$ 0.33	...	...	...
					738.6	...	4.69 $\pm$ 0.21	...	
					1090.7	...	...	6.4 $\pm$ 0.2	
					1172.5	5.87 $\pm$ 0.29	...	...	
					51.9	...	...	<0.58	
					59.4	1.27 $\pm$ 0.35	...	...	
					682.7	...	3.88 $\pm$ 0.19	...	
AT2019azh	2019-02-22T00:28:48	08h13m16.9s	22d38m54s	0.022	1025.3	...	...	...	1.22 $\pm$ 0.22
					1039.8	...	...	2.38 $\pm$ 0.21	
					1127.5	2.83 $\pm$ 0.2	...	...	
					-304.2	...	...	<0.39	
					172.9	<0.69	...	...	
					294.4	<0.78	...	...	
					357.2	<0.81	...	...	
AT2018hyz	2018-11-06T15:21:36	10h06m50.9s	01d41m34s	0.046	358.2	<0.75	...	...	...
					408.2	<0.73	...	...	
					430.1	<0.75	...	...	
					431.1	<0.85	...	...	

**Table 2** continued

Table 2 (continued)

Name	RA	DEC	Discovery (UT)	z	$\delta t$ (days)	RACS low (mJy)	RACS mid (mJy)	RACS high (mJy)	VLA55 (mJy)
				...	436.1	<0.82	...	...	...
				...	437.1	<0.68	...	...	...
				...	438.1	<0.61	...	...	...
				...	591.7	<0.67	...	...	...
				...	661.5	<0.94	...	...	...
				...	676.2	...	...	...	0.54±0.17
				...	795.2	...	0.96±0.21	...	...
				...	988.6	1.23±0.2	...	...	...
				...	1018.5	1.07±0.21	...	...	...
				...	1158.2	...	...	4.85±0.22	...
				...	1240.0	3.58±0.16	...	...	...
				...	1553.8	...	...	...	16.67±2.5
				...	1679.8	8.12±0.18	...	...	...
				...	1701.7	8.43±0.19	...	...	...
				...	1757.5	7.27±0.53	...	...	...
AT2019qiz	2019-09-19T11:59:43	04h46m37.9s	-10d13m35s	0.015	-617.3	...	...	...	<0.36
				...	-142.2	<1.55	...	...	...
				...	396.9	...	...	...	1.1±0.26
				...	490.0	...	1.33±0.17	...	...
				...	841.1	...	...	1.25±0.18	...
				...	938.8	1.19±0.18	...	...	...
				...	1282.5	...	...	...	0.92±0.21
				...	1387.6	<9.31	...	...	...
				...	1445.4	<2.11	...	...	...
AT2020zso	2020-11-12T03:36:05.003	22h22m17.1s	-07d16m00s	0.061	-1080.0	...	...	...	0.99±0.2
				...	-563.2	<0.79	...	...	...
				...	-442.4	<0.91	...	...	...
				...	-379.6	<0.74	...	...	...
				...	-378.7	<0.79	...	...	...
				...	-305.9	<0.79	...	...	...

Table 2 continued



Table 2 (continued)

Name	RA	DEC	Discovery (UT)	z	$\delta t$ (days)	RACS low (mJy)	RACS mid (mJy)	RACS high (mJy)	VLA55 (mJy)
				...	-304.9	<0.89	...	...	...
				...	-298.8	<0.71	...	...	...
				...	-297.8	<0.71	...	...	...
				...	-145.3	<0.72	...	...	...
				...	-124.6	...	...	...	<0.54
				...	-74.5	<0.85	...	...	...
				...	46.2	...	<0.58	...	...
				...	252.7	<0.67	...	...	...
				...	284.5	<0.87	...	...	...
				...	442.1	...	...	<0.62	...
				...	538.8	0.91±0.17	...	...	...
				...	794.8	...	...	...	1.49±0.29
				...	962.7	<1.07	...	...	...
				...	967.7	<0.86	...	...	...
				...	1025.6	<0.83	...	...	...
AT2021qyv	2021-05-10T10:50:52.800	15h18m59.3s	-03d11m45s	0.183	-748.0	...	...	...	<0.59
				...	-741.9	<1.32	...	...	...
				...	-79.5	...	<0.57	...	...
				...	216.2	...	...	...	<0.41
				...	245.6	...	...	<0.6	...
				...	331.3	1.66±0.38	...	...	...
				...	764.2	<1.43	...	...	...
				...	774.1	<1.15	...	...	...
				...	787.1	<1.36	...	...	...
				...	843.9	<1.56	...	...	...
AT2022bdw	2022-01-31T09:37:26.400	08h25m10.4s	18d34m57s	0.038	-1023.4	...	...	...	<0.36
				...	-1014.9	1.04±0.25	...	...	...
				...	-384.7	...	0.63±0.18	...	...
				...	-75.0	...	...	...	<0.35
				...	-30.6	...	...	<0.6	...

Table 2 continued

Table 2 (*continued*)

Name	RA	DEC	Discovery (UT)	z	$\delta t$ (days)	RACS low (mJy)	RACS mid (mJy)	RACS high (mJy)	VLASS (mJy)
AT2022dsb	2022-03-01T13:40:47	15h42m21.7s	-22d40m14s	0.023	56.1	0.91 $\pm$ 0.21	...	...	...
				...	100.0	1.39 $\pm$ 0.19	...	...	...
				0.023	-1475.1	...	...	...	<0.46
				...	-1041.0	1.29 $\pm$ 0.3	...	...	...
				...	-482.8	...	...	...	<0.48
				...	-363.7	...	0.56 $\pm$ 0.16	...	...
				...	-47.5	...	...	<0.65	...
				...	41.2	0.76 $\pm$ 0.21	...	...	...
ASASSN-14li	2014-11-22T00:00:00	12h48m15.2s	17d46m26s	0.021	1602.4	...	...	...	0.58 $\pm$ 0.15
				...	1614.5	2.88 $\pm$ 0.28	...	...	...
				...	2230.0	...	1.54 $\pm$ 0.19	...	...
				...	2552.5	...	...	...	0.77 $\pm$ 0.17
				...	2615.9	...	...	1.3 $\pm$ 0.18	...
				...	2681.7	2.39 $\pm$ 0.2	...	...	...

*Facilities: ASKAP*

## APPENDIX

**Table 3.** Upper limits ( $3\text{-}\sigma$ ) on the radio emission from the RACS/VAST survey for the sample of TDEs that are in RACS footprint but resulted in non-detections.

Name	$\delta t$	Flux limit		Luminosity limit <sup>a</sup>	
		RACS	VAST	RACS	VAST
		(days)	(mJy)	(mJy)	(ergs/s)
AT2016fnl	1121	0.8	...	$4.6 \times 10^{36}$	...
AT2016fnl	2047	0.6	...	$3.5 \times 10^{36}$	...
AT2018dyb	466	2.1	...	$1.5 \times 10^{37}$	...
AT2018dyb	1370	2.4	...	$1.6 \times 10^{37}$	...
AT2018fyk	419	0.6	...	$5.0 \times 10^{37}$	...
AT2018fyk	517	...	0.7	...	$5.4 \times 10^{37}$
AT2018fyk	518	...	0.5	...	$4.4 \times 10^{37}$
AT2018fyk	520	...	0.5	...	$4.2 \times 10^{37}$
AT2018fyk	521	...	0.5	...	$4.3 \times 10^{37}$
AT2018fyk	727	...	0.6	...	$4.9 \times 10^{37}$
AT2018fyk	1024	...	0.5	...	$3.8 \times 10^{37}$
AT2018fyk	1049	...	0.4	...	$3.7 \times 10^{37}$
AT2018fyk	1080	...	0.5	...	$3.7 \times 10^{37}$
AT2018fyk	1334	0.4	...	$3.3 \times 10^{37}$	...
AT2018fyk	1762	...	0.7	...	$5.4 \times 10^{37}$
AT2018fyk	1763	...	0.5	...	$3.9 \times 10^{37}$
AT2018hco	355	1.1	...	$2.2 \times 10^{38}$	...
AT2018hco	1282	0.9	...	$1.6 \times 10^{38}$	...
AT2018iih	320	0.7	...	$9.1 \times 10^{38}$	...
AT2018iih	1241	0.5	...	$6.2 \times 10^{38}$	...
AT2018lna	271	0.8	...	$1.6 \times 10^{38}$	...
AT2018lna	1193	0.6	...	$1.2 \times 10^{38}$	...
AT2018zr	571	0.7	...	$7.8 \times 10^{37}$	...
AT2018zr	1491	0.6	...	$6.5 \times 10^{37}$	...
AT2019bhf	245	1.7	...	$6.1 \times 10^{38}$	...
AT2019bhf	1147	0.8	...	$2.9 \times 10^{38}$	...
AT2019dsg	191	0.9	...	$5.6 \times 10^{37}$	...
AT2019dsg	1095	0.6	...	$3.6 \times 10^{37}$	...
AT2019gte	139	0.8	...	$1.5 \times 10^{38}$	...
AT2019gte	252	...	0.8	...	$1.5 \times 10^{38}$
AT2019gte	252	...	1.0	...	$1.7 \times 10^{38}$

**Table 3** *continued*

**Table 3** (*continued*)

Name	$\delta t$	Flux limit		Luminosity limit <sup>a</sup>	
		RACS	VAST	RACS	VAST
		(days)	(mJy)	(mJy)	(ergs/s)
AT2019gte	254	...	1.0	...	$1.8 \times 10^{38}$
AT2019gte	255	...	0.7	...	$1.2 \times 10^{38}$
AT2019gte	255	...	0.9	...	$1.5 \times 10^{38}$
AT2019gte	462	...	0.8	...	$1.4 \times 10^{38}$
AT2019gte	760	...	0.6	...	$1.1 \times 10^{38}$
AT2019gte	783	...	0.7	...	$1.1 \times 10^{38}$
AT2019gte	814	...	0.7	...	$1.2 \times 10^{38}$
AT2019gte	1037	0.6	...	$1.0 \times 10^{38}$	...
AT2019gte	1484	...	0.6	...	$1.1 \times 10^{38}$
AT2019gte	1497	...	0.9	...	$1.6 \times 10^{38}$
AT2019lwu	86	0.8	...	$2.8 \times 10^{38}$	...
AT2019lwu	197	...	0.9	...	$3.0 \times 10^{38}$
AT2019lwu	198	...	0.9	...	$2.9 \times 10^{38}$
AT2019lwu	200	...	0.8	...	$2.8 \times 10^{38}$
AT2019lwu	200	...	0.9	...	$3.0 \times 10^{38}$
AT2019lwu	201	...	0.7	...	$2.3 \times 10^{38}$
AT2019lwu	201	...	0.7	...	$2.5 \times 10^{38}$
AT2019lwu	407	...	0.9	...	$3.0 \times 10^{38}$
AT2019lwu	706	...	0.8	...	$2.7 \times 10^{38}$
AT2019lwu	730	...	0.8	...	$2.7 \times 10^{38}$
AT2019lwu	760	...	0.7	...	$2.5 \times 10^{38}$
AT2019lwu	1001	0.6	...	$1.9 \times 10^{38}$	...
AT2019lwu	1444	...	0.7	...	$2.5 \times 10^{38}$
AT2019lwu	1444	...	0.8	...	$2.7 \times 10^{38}$
AT2019vcb	-52	0.8	...	$1.4 \times 10^{38}$	...
AT2019vcb	868	0.5	...	$1.0 \times 10^{38}$	...
AT2020acka	-421	3.3	...	$1.2 \times 10^{40}$	...
AT2020acka	479	1.3	...	$4.5 \times 10^{39}$	...
AT2020neh	-247	0.9	...	$7.8 \times 10^{37}$	...
AT2020neh	654	0.6	...	$5.3 \times 10^{37}$	...
AT2020pj	-79	0.6	...	$6.4 \times 10^{37}$	...
AT2020pj	822	0.5	...	$5.2 \times 10^{37}$	...
AT2020vwl	-361	0.7	...	$2.0 \times 10^{37}$	...
AT2020vwl	540	0.5	...	$1.4 \times 10^{37}$	...
AT2021ack	-455	1.1	...	$4.7 \times 10^{38}$	...
AT2021ack	447	1.0	...	$4.5 \times 10^{38}$	...
AT2021ack	484	0.8	...	$3.7 \times 10^{38}$	...
AT2021ack	885	...	1.1	...	$5.1 \times 10^{38}$
AT2021ack	905	...	1.3	...	$5.8 \times 10^{38}$

**Table 3** *continued*

**Table 3** (*continued*)

Name	$\delta t$	Flux limit		Luminosity limit <sup>a</sup>	
		RACS	VAST	RACS	VAST
		(days)	(mJy)	(mJy)	(ergs/s)
AT2021axu	-481	0.6	...	$6.2 \times 10^{38}$	...
AT2021axu	439	0.5	...	$5.0 \times 10^{38}$	...
AT2021blz	-472	0.7	...	$3.3 \times 10^{37}$	...
AT2021blz	445	0.5	...	$2.4 \times 10^{37}$	...
AT2021blz	886	...	0.5	...	$2.3 \times 10^{37}$
AT2021ehb	-487	0.8	...	$5.3 \times 10^{36}$	...
AT2021ehb	397	0.7	...	$4.9 \times 10^{36}$	...
AT2021gje	-504	1.0	...	$4.3 \times 10^{39}$	...
AT2021gje	380	0.6	...	$2.5 \times 10^{39}$	...
AT2021jjm	-540	1.3	...	$7.8 \times 10^{38}$	...
AT2021jjm	365	0.7	...	$4.1 \times 10^{38}$	...
AT2021jsg	-471	0.6	...	$2.3 \times 10^{38}$	...
AT2021jsg	449	0.5	...	$2.0 \times 10^{38}$	...
AT2021lo	-446	1.1	...	$6.4 \times 10^{38}$	...
AT2021lo	460	0.7	...	$3.9 \times 10^{38}$	...
AT2021lo	894	...	0.7	...	$3.9 \times 10^{38}$
AT2021lo	913	...	0.7	...	$4.3 \times 10^{38}$
AT2021mhg	-595	0.8	...	$9.4 \times 10^{37}$	...
AT2021mhg	331	0.6	...	$7.4 \times 10^{37}$	...
AT2021uqv	-674	0.8	...	$2.2 \times 10^{38}$	...
AT2021uqv	253	0.9	...	$2.4 \times 10^{38}$	...
AT2021uvz	-656	0.8	...	$6.6 \times 10^{38}$	...
AT2021uvz	265	0.6	...	$5.2 \times 10^{38}$	...
AT2021yte	-719	0.8	...	$5.1 \times 10^{37}$	...
AT2021yte	218	0.6	...	$3.7 \times 10^{37}$	...
AT2021yte	234	0.5	...	$3.4 \times 10^{37}$	...
AT2021yzv	-655	0.9	...	$2.3 \times 10^{39}$	...
AT2021yzv	228	0.8	...	$2.0 \times 10^{39}$	...
AT2022adm	-829	1.6	...	$1.4 \times 10^{38}$	...
AT2022adm	72	0.7	...	$6.3 \times 10^{37}$	...
AT2022arb	-833	1.0	...	$8.7 \times 10^{37}$	...
AT2022arb	-725	...	1.0	...	$8.8 \times 10^{37}$
AT2022arb	-721	...	1.1	...	$9.6 \times 10^{37}$
AT2022arb	-721	...	1.2	...	$1.0 \times 10^{38}$
AT2022arb	-720	...	0.9	...	$8.1 \times 10^{37}$
AT2022arb	-720	...	1.3	...	$1.2 \times 10^{38}$
AT2022arb	-719	...	4.0	...	$3.5 \times 10^{38}$
AT2022arb	-718	...	0.8	...	$7.4 \times 10^{37}$
AT2022arb	-718	...	1.2	...	$1.1 \times 10^{38}$

**Table 3** *continued*

Table 3 (continued)

Name	$\delta t$	Flux limit		Luminosity limit <sup>a</sup>	
		RACS	VAST	RACS	VAST
	(days)	(mJy)	(mJy)	(ergs/s)	(ergs/s)
AT2022arb	−703	...	3.9	...	$3.4 \times 10^{38}$
AT2022arb	−512	...	3.8	...	$3.4 \times 10^{38}$
AT2022arb	−213	...	0.9	...	$7.9 \times 10^{37}$
AT2022arb	−190	...	0.7	...	$6.5 \times 10^{37}$
AT2022arb	−160	...	0.9	...	$7.5 \times 10^{37}$
AT2022arb	66	0.6	...	$5.4 \times 10^{37}$	...
AT2022arb	504	...	0.7	...	$6.0 \times 10^{37}$
AT2022arb	524	...	0.8	...	$7.5 \times 10^{37}$
AT2022czy	−843	0.9	...	$2.7 \times 10^{38}$	...
AT2022czy	39	0.7	...	$1.9 \times 10^{38}$	...
AT2022dyt	−885	0.7	...	$8.3 \times 10^{37}$	...
AT2022dyt	33	0.6	...	$7.0 \times 10^{37}$	...
AT2022exr	−887	0.7	...	$1.6 \times 10^{38}$	...
AT2022exr	14	0.6	...	$1.2 \times 10^{38}$	...

<sup>a</sup>Radio luminosity is estimated as  $\nu L_\nu$  and we assume the emission to be spherical which results in the inclusion of  $4\pi$  factor.

## REFERENCES

- Alexander, K. D., Berger, E., Guillochon, J., Zauderer, B. A., & Williams, P. K. G. 2016, *ApJL*, 819, L25, doi: [10.3847/2041-8205/819/2/L25](https://doi.org/10.3847/2041-8205/819/2/L25)
- Alexander, K. D., van Velzen, S., Horesh, A., & Zauderer, B. A. 2020, *SSRv*, 216, 81, doi: [10.1007/s11214-020-00702-w](https://doi.org/10.1007/s11214-020-00702-w)
- Alexander, K. D., Velzen, S. v., Miller-Jones, J., et al. 2021, *The Astronomer’s Telegram*, 14337, 1
- Anderson, M. M., Mooley, K. P., Hallinan, G., et al. 2020, *ApJ*, 903, 116, doi: [10.3847/1538-4357/abb94b](https://doi.org/10.3847/1538-4357/abb94b)
- Andreoni, I., Coughlin, M. W., Perley, D. A., et al. 2022, *Nature*, 612, 430, doi: [10.1038/s41586-022-05465-8](https://doi.org/10.1038/s41586-022-05465-8)
- Auchettl, K., Guillochon, J., & Ramirez-Ruiz, E. 2017, *ApJ*, 838, 149, doi: [10.3847/1538-4357/aa633b](https://doi.org/10.3847/1538-4357/aa633b)
- Barniol Duran, R., Nakar, E., & Piran, T. 2013, *ApJ*, 772, 78, doi: [10.1088/0004-637X/772/1/78](https://doi.org/10.1088/0004-637X/772/1/78)
- Bellm, E. C., Kulkarni, S. R., Graham, M. J., et al. 2019, *PASP*, 131, 018002, doi: [10.1088/1538-3873/aaecbe](https://doi.org/10.1088/1538-3873/aaecbe)
- Bright, J. S., Fender, R. P., Motta, S. E., et al. 2018, *MNRAS*, 475, 4011, doi: [10.1093/mnras/sty077](https://doi.org/10.1093/mnras/sty077)
- Cendes, Y., Berger, E., Alexander, K. D., et al. 2022, *ApJ*, 938, 28, doi: [10.3847/1538-4357/ac88d0](https://doi.org/10.3847/1538-4357/ac88d0)
- . 2023, arXiv e-prints, arXiv:2308.13595, doi: [10.48550/arXiv.2308.13595](https://doi.org/10.48550/arXiv.2308.13595)
- Chevalier, R. A. 1998, *ApJ*, 499, 810, doi: [10.1086/305676](https://doi.org/10.1086/305676)
- Christy, C. T., Alexander, K. D., Cendes, Y., et al. 2024, arXiv e-prints, arXiv:2404.12431, doi: [10.48550/arXiv.2404.12431](https://doi.org/10.48550/arXiv.2404.12431)
- Condon, J. J., Cotton, W. D., & Broderick, J. J. 2002, *AJ*, 124, 675, doi: [10.1086/341650](https://doi.org/10.1086/341650)
- Duchesne, S. W., Thomson, A. J. M., Pritchard, J., et al. 2023, *PASA*, 40, e034, doi: [10.1017/pasa.2023.31](https://doi.org/10.1017/pasa.2023.31)
- Dykaar et al. 2024, in prep.
- Forster, F., Bauer, F. E., Munoz-Arancibia, A., et al. 2020, *Transient Name Server Discovery Report*, 2020-3449, 1
- Gehrels, N. 1986, *ApJ*, 303, 336, doi: [10.1086/164079](https://doi.org/10.1086/164079)
- Gezari, S. 2021, *ARA&A*, 59, 21, doi: [10.1146/annurev-astro-111720-030029](https://doi.org/10.1146/annurev-astro-111720-030029)
- Goodwin, A., Anderson, G., Miller-Jones, J., et al. 2022a, *The Astronomer’s Telegram*, 15293, 1

- Goodwin, A. J., van Velzen, S., Miller-Jones, J. C. A., et al. 2022b, *MNRAS*, 511, 5328, doi: [10.1093/mnras/stac333](https://doi.org/10.1093/mnras/stac333)
- Granot, J., & Sari, R. 2002, *ApJ*, 568, 820, doi: [10.1086/338966](https://doi.org/10.1086/338966)
- Guzman, J., Whiting, M., Voronkov, M., et al. 2019, ASKAPsoft: ASKAP science data processor software. <http://ascl.net/1912.003>
- Hale, C. L., McConnell, D., Thomson, A. J. M., et al. 2021, *PASA*, 38, e058, doi: [10.1017/pasa.2021.47](https://doi.org/10.1017/pasa.2021.47)
- Halpern, J. P., Gezari, S., & Komossa, S. 2004, *ApJ*, 604, 572, doi: [10.1086/381937](https://doi.org/10.1086/381937)
- Hammerstein, E., van Velzen, S., Gezari, S., et al. 2023, *ApJ*, 942, 9, doi: [10.3847/1538-4357/aca283](https://doi.org/10.3847/1538-4357/aca283)
- Holoien, T. W. S., Kochanek, C. S., Prieto, J. L., et al. 2016, *MNRAS*, 463, 3813, doi: [10.1093/mnras/stw2272](https://doi.org/10.1093/mnras/stw2272)
- Holoien, T. W. S., Valley, P. J., Auchettl, K., et al. 2019, *ApJ*, 883, 111, doi: [10.3847/1538-4357/ab3c66](https://doi.org/10.3847/1538-4357/ab3c66)
- Horesh, A., Cenko, S. B., & Arcavi, I. 2021, *Nature Astronomy*, 5, 491, doi: [10.1038/s41550-021-01300-8](https://doi.org/10.1038/s41550-021-01300-8)
- Horesh, A., Burger, N., Sfaradi, I., et al. 2022, *The Astronomer's Telegram*, 15307, 1
- Hotan, A. W., Bunton, J. D., Chippendale, A. P., et al. 2021, *PASA*, 38, e009, doi: [10.1017/pasa.2021.1](https://doi.org/10.1017/pasa.2021.1)
- Hung, T., Foley, R. J., Veilleux, S., et al. 2021, *ApJ*, 917, 9, doi: [10.3847/1538-4357/abf4c3](https://doi.org/10.3847/1538-4357/abf4c3)
- Jauncey, D. L., Bignall, H. E., Kedziora-Chudczer, L., et al. 2016, *Galaxies*, 4, 62, doi: [10.3390/galaxies4040062](https://doi.org/10.3390/galaxies4040062)
- Jiang, N., Wang, T., Hu, X., et al. 2021, *ApJ*, 911, 31, doi: [10.3847/1538-4357/abe772](https://doi.org/10.3847/1538-4357/abe772)
- Jones, D. O., French, K. D., Agnello, A., et al. 2021, *Transient Name Server Discovery Report*, 2021-2199, 1
- Jose, J., Guo, Z., Long, F., et al. 2014, *The Astronomer's Telegram*, 6777, 1
- Krolik, J., Piran, T., Svirski, G., & Cheng, R. M. 2016, *ApJ*, 827, 127, doi: [10.3847/0004-637X/827/2/127](https://doi.org/10.3847/0004-637X/827/2/127)
- Lacy, M., Baum, S. A., Chandler, C. J., et al. 2020, *PASP*, 132, 035001, doi: [10.1088/1538-3873/ab63eb](https://doi.org/10.1088/1538-3873/ab63eb)
- Leung, J. K., Murphy, T., Lenc, E., et al. 2023, *MNRAS*, 523, 4029, doi: [10.1093/mnras/stad1670](https://doi.org/10.1093/mnras/stad1670)
- Masterson, M., De, K., Panagiotou, C., et al. 2024, *ApJ*, 961, 211, doi: [10.3847/1538-4357/ad18bb](https://doi.org/10.3847/1538-4357/ad18bb)
- Matsumoto, T., & Piran, T. 2023, *MNRAS*, 522, 4565, doi: [10.1093/mnras/stad1269](https://doi.org/10.1093/mnras/stad1269)
- McConnell, D., Hale, C. L., Lenc, E., et al. 2020, *PASA*, 37, e048, doi: [10.1017/pasa.2020.41](https://doi.org/10.1017/pasa.2020.41)
- Murphy, T., Chatterjee, S., Kaplan, D. L., et al. 2013, *PASA*, 30, e006, doi: [10.1017/pasa.2012.006](https://doi.org/10.1017/pasa.2012.006)
- Murphy, T., Kaplan, D. L., Stewart, A. J., et al. 2021, *PASA*, 38, e054, doi: [10.1017/pasa.2021.44](https://doi.org/10.1017/pasa.2021.44)
- Nakar, E., & Piran, T. 2011, *Nature*, 478, 82, doi: [10.1038/nature10365](https://doi.org/10.1038/nature10365)
- Nicholl, M., Wevers, T., Oates, S. R., et al. 2020, *MNRAS*, 499, 482, doi: [10.1093/mnras/staa2824](https://doi.org/10.1093/mnras/staa2824)
- O'Brien, A., Kaplan, D., Murphy, T., Yu, W., & Zhang, W. 2019a, *The Astronomer's Telegram*, 13310, 1
- . 2019b, *The Astronomer's Telegram*, 13334, 1
- Pacholczyk, A. G. 1970, *Radio astrophysics. Nonthermal processes in galactic and extragalactic sources*
- Pasham, D. R., & van Velzen, S. 2018, *ApJ*, 856, 1, doi: [10.3847/1538-4357/aab361](https://doi.org/10.3847/1538-4357/aab361)
- Patra, K. C., Lu, W., Brink, T. G., et al. 2022, *MNRAS*, 515, 138, doi: [10.1093/mnras/stac1727](https://doi.org/10.1093/mnras/stac1727)
- Planck Collaboration, Aghanim, N., Akrami, Y., et al. 2020, *A&A*, 641, A6, doi: [10.1051/0004-6361/201833910](https://doi.org/10.1051/0004-6361/201833910)
- Pritchard, J., Murphy, T., Heald, G., et al. 2024, *MNRAS*, doi: [10.1093/mnras/stae127](https://doi.org/10.1093/mnras/stae127)
- Ravi, V., Dykaar, H., Codd, J., et al. 2022, *ApJ*, 925, 220, doi: [10.3847/1538-4357/ac2b33](https://doi.org/10.3847/1538-4357/ac2b33)
- Rees, M. J. 1988, *Nature*, 333, 523, doi: [10.1038/333523a0](https://doi.org/10.1038/333523a0)
- Roy, R., Nayana, A. J., & Chandra, P. 2021, *The Astronomer's Telegram*, 14828, 1
- Sabater, J., Best, P. N., Hardcastle, M. J., et al. 2019, *A&A*, 622, A17, doi: [10.1051/0004-6361/201833883](https://doi.org/10.1051/0004-6361/201833883)
- Sfaradi, I., Horesh, A., Bright, J., et al. 2023, *The Astronomer's Telegram*, 15918, 1
- Sfaradi, I., Horesh, A., Fender, R., et al. 2022, *ApJ*, 933, 176, doi: [10.3847/1538-4357/ac74bc](https://doi.org/10.3847/1538-4357/ac74bc)
- Sfaradi, I., Beniamini, P., Horesh, A., et al. 2024, *MNRAS*, 527, 7672, doi: [10.1093/mnras/stad3717](https://doi.org/10.1093/mnras/stad3717)
- Shappee, B. J., Prieto, J. L., Grupe, D., et al. 2014, *ApJ*, 788, 48, doi: [10.1088/0004-637X/788/1/48](https://doi.org/10.1088/0004-637X/788/1/48)
- Siebert, M. R., Strasburger, E., Rojas-Bravo, C., & Foley, R. J. 2019, *The Astronomer's Telegram*, 13131, 1
- Somalwar, J. J., Ravi, V., Dong, D. Z., et al. 2023, *ApJ*, 945, 142, doi: [10.3847/1538-4357/acbafc](https://doi.org/10.3847/1538-4357/acbafc)
- Stanek, K. Z. 2023, *Transient Name Server Discovery Report*, 2023-421, 1
- Stanek, K. Z., & Kochanek, C. S. 2022, *Transient Name Server Discovery Report*, 2022-559, 1
- Tonry, J., Denneau, L., Weiland, H., et al. 2022, *Transient Name Server Discovery Report*, 2022-284, 1
- van Velzen, S., Holoien, T. W. S., Onori, F., Hung, T., & Arcavi, I. 2020, *SSRv*, 216, 124, doi: [10.1007/s11214-020-00753-z](https://doi.org/10.1007/s11214-020-00753-z)
- van Velzen, S., Mendez, A. J., Krolik, J. H., & Gorjian, V. 2016, *ApJ*, 829, 19, doi: [10.3847/0004-637X/829/1/19](https://doi.org/10.3847/0004-637X/829/1/19)
- van Velzen, S., Pasham, D. R., Komossa, S., Yan, L., & Kara, E. A. 2021, *SSRv*, 217, 63, doi: [10.1007/s11214-021-00835-6](https://doi.org/10.1007/s11214-021-00835-6)

Wright, E. L., Eisenhardt, P. R. M., Mainzer, A. K., et al. 2010, *AJ*, 140, 1868, doi: [10.1088/0004-6256/140/6/1868](https://doi.org/10.1088/0004-6256/140/6/1868)  
Yao, Y., Ravi, V., Gezari, S., et al. 2023, *ApJL*, 955, L6, doi: [10.3847/2041-8213/acf216](https://doi.org/10.3847/2041-8213/acf216)

Zauderer, B. A., Berger, E., Soderberg, A. M., et al. 2011, *Nature*, 476, 425, doi: [10.1038/nature10366](https://doi.org/10.1038/nature10366)